DRAFT

To be submitted to *AJ*

HNBody: A Symplectic Integration Package for Nearly-Keplerian Systems — I. Systems Without Close Encounters

Kevin P. Rauch[1] and Douglas P. Hamilton[2]

Department of Astronomy, University of Maryland, College Park, MD 20742-2421

ABSTRACT

We describe a new software package, HNBody, for simulating the dynamical evolution of hierarchical (i.e., nearly-Keplerian) N-body systems. The main algorithms are based on Wisdom-Holman type symplectic methods, in which Keplerian motion is treated exactly. Native support is included for second and fourth order methods, symplectic correctors, post-Newtonian corrections, and others. Particles may be assigned to one of three mass classes (heavy, light, and zeroweight); zeroweight particles comprise a semi-independent subsystem and may be integrated using a different coordinate system and/or time step than the other bodies. Our implementation features efficient roundoff control which can reduce finite-precision artifacts by several orders of magnitude, with negligible increase in run time ($< 10\%$). Integrations are initialized via input files employing a flexible keyword-based interface. As one of several sample applications, we apply HNBody to the classic problem of the long-term evolution of the Solar System, including a 10 Gyr run modeling the Moon as a quadrupole perturbation, and a 200 Myr run in which the Moon is explicitly resolved. We compare our results with the JPL DE406 ephemeris and with a recent best-of-class Störmer calculation extending over 50 Myr into the past; excellent agreement with both is found. We also conclude that the Wisdom-Holman method remains an order of magnitude more efficient than Störmer methods even for high-precision, roundoff-limited Solar System integrations.

Subject headings: celestial mechanics — ephemerides — methods: numerical — solar system: general

1. INTEGRATION OF NEARLY-KEPLERIAN SYSTEMS

Symplectic integration schemes have become highly popular tools for the numerical study of dynamical systems, a result of their often high efficiency as well as their typical long-term stability

[1]rauch@astro.umd.edu

[2]hamilton@astro.umd.edu

(see, e.g., Marsden, Patrick, & Shadwick (1996) and the many references within)....

2. THE HNBODY PACKAGE

The effort required to turn an abstract computational algorithm into a practical and reliable numerical method can be a significant barrier to its widespread use (and hence usefulness). In principle explicit symplectic integrators such as leap frog and the basic Kepler mappings are easily programmed; however, implementing an efficient and reliable Kepler stepper and extensions such as symplectic correctors, etc., require major additional investments of time that most researchers cannot afford. In addition, variations in the coding of numerical details will affect performance; for high precision calculations in particular, this can obscure whether systematic differences observed between two particular algorithms are inherent to the methods or instead are implementation artifacts.

The purpose of HNBody [1] is to provide an extensible symplectic integration infrastructure enabling convenient, selective use of a variety of integration algorithms and physical processes. Although our primary focus is on Kepler mappings, two generic ODE integrators—Runge-Kutta and Bulirsch-Stoer—are also available. In coding the algorithms, careful attention has been paid to maintaining maximum numerical accuracy, in order to make our implementation as 'transparent' (close to ideal) as possible within the limits imposed by double-precision computer arithmetic. This has been accomplished without significantly reducing performance. At the software level, modern coding standards and development tools (e.g., CVS, autoconf, doxygen) have been used to produce a maintainable, stable, and well-tested code base.

Performing a simulation with HNBody involves creating a plain text options file containing keywords describing the integration (number of particles, initial conditions, integration stepsize, and so on); this is then supplied as input to a driver program which carries out the specified simulation. The package includes a default driver program supporting the baseline functionality and physical effects described below, and is organized such that additional physics (non-gravitational forces, etc.) can be added easily to a particular simulation through creation of a custom driver. This arrangement allows straightforward integrations to be performed very quickly (without writing or compiling code), while also providing the flexibility required to simulate more complicated systems.

The following sections detail the architecture and current capabilities of HNBody. We focus on precise definitions of the mathematical equations underlying each algorithm rather than a tutorial-style exposition (user-level documentation is available in the download package and on our web site).

---

[1] http://janus.astro.umd.edu/HNBody/

2.1. Integration Methods

2.1.1. Symplectic Methods

The performance of a symplectic integrator depends on both the form of the Hamiltonian describing the system, and how it is divided into pieces to produce a practical algorithm. Consider a generic Hamiltonian $\mathcal{H} = \mathcal{H}(\mathbf{q}, \mathbf{p})$, where $\mathbf{q}$ and $\mathbf{p}$ are generalized position and momentum vectors, respectively. An arbitrary splitting of $\mathcal{H}$ into pieces can be written in the form

$$\mathcal{H} = \mathcal{H}_0 + \mathcal{K}(\mathbf{q}) + \mathcal{S}(\mathbf{p}) + \sum_i \mathcal{D}_i(\mathbf{q}, \mathbf{p}). \tag{1}$$

The constant term $\mathcal{H}_0$ does not affect the equations of motion and can be neglected. The Hamiltonian piece $\mathcal{K}(\mathbf{q})$ is called the 'kick' term as the equations of motion $\dot{\mathbf{p}} = -\nabla_{\mathbf{q}}\mathcal{K}$ alter only the momentum component. We refer to $\mathcal{S}(\mathbf{p})$ as the 'shift' term since the equations of motion $\dot{\mathbf{q}} = +\nabla_{\mathbf{p}}\mathcal{S}$ change the position vector at fixed momentum. The 'drift' term(s) $\mathcal{D}_i$ evolve multiple position and momentum components simultaneously and are the most critical to the performance of the algorithm in that finding tractable (easily integrated) drift terms can be a challenging task. The essence of the Wisdom-Holman mapping, for example, is to choose a representation $\mathcal{H}$ of the gravitational N-body problem for which the drift terms can be efficiently advanced in time. In contrast, the dynamics produced by kick and shift terms are straightforward to calculate; the leap frog algorithm corresponds to the special case where *no* drift terms are present in Eq. (1).

HNBody can simulate the evolution of any nearly-Keplerian system of particles governed by a Hamiltonian of the form

$$\mathcal{H} = \mathcal{H}_0 + \mathcal{K}(\mathbf{x}) + \mathcal{S}(\mathbf{v}) + \mathcal{D}_{\rm Kep}(\mathbf{x}, \mathbf{v}) + \mathcal{D}_{\rm Misc}(\mathbf{x}, \mathbf{v}), \tag{2}$$

where

$$\mathcal{K}(\mathbf{x}) = \mathcal{K}_{\rm Kep} + \mathcal{K}_{\rm OB} + \mathcal{K}_{\rm PN} + \mathcal{K}_{\rm Misc}, \tag{3}$$

$$\mathcal{S}(\mathbf{v}) = \mathcal{S}_{\rm Kep} + \mathcal{S}_{\rm PN} + \mathcal{S}_{\rm Misc}, \tag{4}$$

and $\mathbf{x}$ and $\mathbf{v}$ are the particle positions and velocities. Here $\mathcal{D}_{\rm Kep}$, $\mathcal{K}_{\rm Kep}$, and $\mathcal{S}_{\rm Kep}$ are respectively the drift, kick, and shift components of the Kepler (N-body) Hamiltonian; $\mathcal{K}_{\rm OB}$ implements oblateness corrections; $\mathcal{K}_{\rm PN}$ and $\mathcal{S}_{\rm PN}$ implement post-Newtonian corrections. The latter two effects are optional and can be selected via input options. The $\mathcal{D}_{\rm Misc}$, $\mathcal{K}_{\rm Misc}$ and $\mathcal{S}_{\rm Misc}$ terms represent arbitrary additional dynamics which can be implemented by the user through creation of a custom driver program. The mathematical form of each term will be defined in the following sections.

The error Hamiltonian for a symplectic method—and hence order of convergence as a function of step size—is determined by both the chosen partitioning of the Hamiltonian and the manner in which the pieces are interleaved to advance the system one time step. Defining a time-advance operator $\mathcal{H}[\Delta t]$ which evolves the phase space coordinates $(\mathbf{q}, \mathbf{p})$ through a time Δt for a physical system defined by $\mathcal{H} = \mathcal{H}(\mathbf{q}, \mathbf{p})$, consider as an example the Hamiltonian $\mathcal{H} = \mathcal{K}(\mathbf{q}) + \mathcal{S}(\mathbf{p})$. Then

both $\mathcal{K}[\Delta t/2]\ \mathcal{S}[\Delta t]\ \mathcal{K}[\Delta t/2]$ and $\mathcal{S}[\Delta t/2]\ \mathcal{K}[\Delta t]\ \mathcal{S}[\Delta t/2]$ define valid but *different* second-order leap frog algorithms for advancing the system $\mathcal{H}$ by a time Δt. Higher-order methods can be constructed through composition of the basic second-order step, as well as other means (...).

HNBody supports both second- and fourth-order symplectic algorithms as well as three interleaving variations; each can be specified via runtime input options. The interleaving choices are called **Drift-Kick**, **Kick-Drift**, and **Shift-Drift** and determine the ordering of Hamiltonian pieces as follows: for option **Drift-Kick** the second-order base step is

$$\mathcal{D}_{\rm Kep}[\Delta t/2]\ \mathcal{D}_{\rm Misc}[\Delta t/2]\ \mathcal{S}[\Delta t/2]\ \mathcal{K}[\Delta t]\ \mathcal{S}[\Delta t/2]\ \mathcal{D}_{\rm Misc}[\Delta t/2]\ \mathcal{D}_{\rm Kep}[\Delta t/2]\ , \tag{5}$$

for **Kick-Drift** it is

$$\mathcal{K}[\Delta t/2]\ \mathcal{S}[\Delta t/2]\ \mathcal{D}_{\rm Misc}[\Delta t/2]\ \mathcal{D}_{\rm Kep}[\Delta t]\ \mathcal{D}_{\rm Misc}[\Delta t/2]\ \mathcal{S}[\Delta t/2]\ \mathcal{K}[\Delta t/2]\ , \tag{6}$$

and for **Shift-Drift** it is

$$\mathcal{S}[\Delta t/2]\ \mathcal{K}[\Delta t/2]\ \mathcal{D}_{\rm Misc}[\Delta t/2]\ \mathcal{D}_{\rm Kep}[\Delta t]\ \mathcal{D}_{\rm Misc}[\Delta t/2]\ \mathcal{K}[\Delta t/2]\ \mathcal{S}[\Delta t/2]\ . \tag{7}$$

Fourth-order mappings are implemented by composing three second-order steps with different timesteps according to

$$\mathcal{H}_{\mathbf{4}}[\Delta t] = \mathcal{H}_{\mathbf{2}}[\alpha\Delta t]\ \mathcal{H}_{\mathbf{2}}[\beta\Delta t]\ \mathcal{H}_{\mathbf{2}}[\alpha\Delta t]\ , \tag{8}$$

where $\alpha = 1/(2-2^{1/3})$ and $\beta = -2^{1/3}/(2-2^{1/3})$ (Yoshida 1990). Our implementation of both second- and fourth-order mappings combine adjacent sub-steps where possible to maximize efficiency during an extended integration (e.g., in Eq. (5) the trailing $\mathcal{D}_{\rm Kep}[\Delta t/2]$ term for one step is automatically combined with the leading drift term of the following step).

2.1.2. ODE Methods

As a debugging aid, and to provide a generic alternative integrator for performing comparative simulations, HNBody also provides two general-purpose numerical integrators based on the Runge-Kutta and Bulirsch-Stoer methods (e.g., Press et al. 1992). We have developed a custom implementation of these basic algorithms incorporating advanced round-off control and other features to facilitate their use with HNBody. Support for oblateness terms and post-Newtonian corrections is also available with these methods, as is the ability to add arbitrary additional forces to a calculation by creating a custom driver program.

Round-off control was implemented in both the symplectic and ODE integrators by augmenting the primary position and velocity vectors $\mathbf{x}$ and $\mathbf{v}$ with residual coordinate vectors $\delta\mathbf{x}$ and $\delta\mathbf{v}$, where the full-precision phase space coordinates are $(\mathbf{x}+\delta\mathbf{x}, \mathbf{v}+\delta\mathbf{v})$. Algorithms were then coded such that the (generally small) changes in particle coordinates suffered during an integration step are accumulated directly into the residual vectors $\delta\mathbf{x}$ and $\delta\mathbf{v}$. After each step the vectors are renormalized using the Kahan summation formula (Goldberg 1991) to make $|\delta\mathbf{x}/\mathbf{x}| \lesssim 10^{-16}$ (assuming

double-precision arithmetic) without altering the numerical sum $\mathbf{x} + \delta\mathbf{x}$. In practical simulations—such as the long-term Solar System integrations presented in § (3.4)—this method was found to reduce round-off by several orders of magnitude, with only a minor performance penalty ($\lesssim 10\%$).

2.2. Particle Classes

N-body systems often contain bodies with a wide range of masses. In the Solar System, for example, $M_\odot \gg M_\mathrm{P} \gg M_\mathrm{A}$, where $M_\odot$, M_P and M_A are the masses of the Sun, planets, and asteroids, respectively. This hierarchy of mass (gravitational potential) between particle types provides an opportunity to increase simulation efficiency by removing Hamiltonian terms with negligible impact on the overall dynamics, such as the self-gravity of the asteroids in the previous example.

HNBody provides explicit support for a three-level mass hierarchy consisting of heavyweight, lightweight, and zeroweight particles (HWPs, LWPs, and ZWPs, respectively). Heavyweight particles—of which there is always at least one (the dominant central mass)—form a fully self-consistent dynamical subsystem. For LWPs, self-gravity (LWP-LWP forces) is ignored; otherwise they are dynamically equivalent to HWPs (HWP-LWP interactions are included). Zeroweight particles comprise a semi-independent subsystem of bodies, each of which is integrated as a perturbed two-body problem, with perturbations due to HWPs and (optionally) LWPs automatically included; ZWPs themselves perturb no other bodies and thus are effectively massless. Note however that HWPs and LWPs may also be massless (assigned zero mass).

Two unique features of ZWPs are the ability to utilize a different step size than the primary HWP-LWP integration, and the option to perform the integration using time-regularized coordinates (Mikkola 1997), which greatly improves the stability of the Kepler mapping for highly eccentric orbits (Rauch & Holman 1999). Quadratic interpolation of HWP-LWP coordinates at times intermediate to the HWP-LWP time step is performed when needed to calculate the ZWP perturbations. These capabilities are particularly useful for systems consisting of widely separated components; for example, a simulation of Kuiper belt objects including perturbations by the Jovian planets could utilize a significantly larger time step for the ZWPs (Kuiper belt) than the HWPs (planets), considerably decreasing the simulation's total running time.

2.3. Coordinate Systems

HNBody provides several different integration (i.e., Hamiltonian) coordinates under which to perform the simulations; the available choices vary with....

2.4. Symplectic Correctors

2.5. Optional Hamiltonian Terms

2.5.1. J_2 and J_4 Oblateness Corrections

2.5.2. Post Newtonian Corrections

2.6. Input/Output Facilities

2.7. Customization

3. COMPARATIVE ANALYSES

The input files defining these tests are available on the HNBody website.

3.1. Jacobi Constant

3.2. Two Jupiters

3.3. Resonance Trapping in the Kuiper Belt

3.4. Long-Term Evolution of the Solar System

Investigation of the long-term stability and evolution of our Solar System is a classic endeavor for which the Kepler mapping is ideally suited. Such simulations remain timely for several reasons. One is the growing number of extra-solar planetary systems being found observationally, several of which display intriguing variations on the dynamics observed in the Solar System (REFS). Advancing interest in the impact of orbital variations on Earth's climate (Varadi, Runnegar, & Ghil 2003, and references therein) and the true value (and consequences) of the Sun's quadrupole moment (Pireaux & Rozelot 2003) are additional examples. Equally important is the availability of published results calculated using a variety of numerical methods and encompassing a range of accuracies and timescales, which allow us to undertake a rigorous comparative analysis of the performance of the symplectic algorithms as implemented by HNBody.

Analytic secular theory (REF), which treats the planets as smooth, massive ellipses instead of discrete particles, predicts (to first-order in eccentricities and inclinations) that the Solar System is stable, and can provide a great deal of insight into the dynamics of well-ordered systems such as our own (REF). As higher-order extensions quickly become unwieldy, however, studying in detail the dynamics of even (apparently) quiescent systems quickly becomes a numerical task; a prime example is the discovery that Pluto's motion is chaotic (Sussman & Wisdom 1988). Two basic computational models can be used—a numerical secular approach, and a direct, particle-based ap-

proach; simplistically, the trade-off between them is (as usual) speed vs. accuracy. Both have been applied to the problem at hand; see, e.g., [Laskar...] and references within for a discussion of the secular method, and Sussman & Wisdom (1992), Quinn, Tremaine, & Duncan (1991), and Applegate et al. (1986) for three examples of direct particle integrations—all using different algorithms. HNBody is of course particle-based, and we limit our comparisons to this class. Some comparison of the direct and secular methods can be found in Varadi et al. (2003).

3.4.1. Numerical Models

We analyze the performance of HNBody applied to this problem using several models that can be directly compared to previous works; these are listed in Table 1. The models are named after the corresponding driver programs used to compute them (supplied as part of the standard distribution). The models differ in their physical accuracy (especially their treatment of the Moon), their numerical accuracy (i.e. truncation error), and the length of the integration. As shown below, the differences in numerical accuracy are noticeable only for Mercury. All models include the nine planets as explicit bodies (HWPs, to be precise) as well as the leading order general relativistic corrections due to the Sun, incorporated as described in section 2.5.2. Planet masses include the mass of their satellites, and positions and velocities refer to the barycenter of the combined system. The constants and initial conditions used are those from the JPL ephemeris DE 405 (Standish 1998), the most accurate general ephemeris currently available (the more recent and special-purpose DE 410 ephemeris—see Standish (2003)—covers only the years 1901 through 2019). The initial epoch was the same as DE 405, JD 2440400.5 (1969 June 28).

Model QTD duplicates the physical model used by Quinn et al. (1991), which accounts for the Moon's influence on the net motion of the Earth-Moon barycenter through inclusion of a mean lunar quadrupole potential. The potential includes an overall scale factor $f \sim 1$ to correct for details of the orbital geometry, to which the authors assign the value $f = 0.9473$. Recession of the lunar orbit due to tidal dissipation is also included in this model; note that we did not include this process in any other models since its effect on the barycenter motion is quite small (it amounts to a very slowly varying value for f) and since it breaks energy conservation, a useful indicator of long-term integrator stability. Model Lunar is similar to QTD except that $f = 0.8525$ is used, the value advocated by Varadi et al. (2003) as most suitable (accurate) for long-term integrations; this model also uses a somewhat smaller stepsize, and neglects tidal effects. Model Lunar+Big3 is identical to Lunar except that the Big 3 asteroids (Ceres, Pallas, and Vesta) are added, and again the stepsize is reduced.

Model EMS+Big3 is analogous to Lunar+Big3 except that the Moon is included as an explicit body instead of a mean potential. It was not, however, treated simply as an extra "planet"; this would be impractical with a standard mapping since the Moon's orbit relative to the Sun is not nearly-Keplerian. Instead, a sub-integration was used in which the Earth-Moon-Sun subsystem was treated self-consistently (hence the moniker EMS), with the remaining planets treating the Earth-

Moon barycenter (as computed by the sub-integration) as a single particle, just as in the other models. Technical details of this procedure can be found in section A.1. Finally, model EMS+J_2 is similar to EMS+Big3 with asteroids replaced by a non-zero Solar quadrupole moment; the value used, $J_2 = 2 \times 10^{-7}$, is commensurate with current estimates (Pireaux & Rozelot 2003; Roxburgh 2001; Pijpers 1998). Note that models EMS+Big3 and EMS+J_2 used a fourth-order mapping (and a corresponding symplectic corrector), so that truncation errors in these models are much smaller than for the others—-which used the usual second-order mapping—-in spite of their only modestly reduced step size.

We assessed the physical accuracy of each model by comparing its output with the DE 406 ephemeris, the extension of DE 405 spanning the date range 3000 B.C. to 3000 A.D. The relative differences for each planet are listed in Table 2 in terms of mean linear and quadratic growth rates (α and β, respectively) in their positional errors relative to DE 406; velocity errors were proportionate. Note that the values provided are neither formal least-squares fits (local averages were used), nor do they represent tight relations (although the amplitude of oscillation about the mean trend was typically a few times smaller than the value of α); however, they reproduce the average trends quite well. The sign of the deviation indicates whether the error was in the leading (+) or trailing (-) hemisphere defined by the body's local velocity $\mathbf{V}$. For all models and bodies (except the Moon) the positional error $\delta\mathbf{X} = \mathbf{X} - \mathbf{X}_{406}$ was nearly aligned with $\mathbf{V}$ (either parallel or anti-parallel); hence offsets were mainly in orbital phase, with $\delta\mathbf{X} \cdot \mathbf{V} > 0$ indicating an advanced phase relative to DE 406 and $\delta\mathbf{X} \cdot \mathbf{V} < 0$ indicating retarded phase.

We can draw a number of conclusions from Table 2 regarding both the leading source of error for each model, and their absolute accuracy relative to the uncertainties of DE 406 itself (whether due to observational or modeling limitations). For Mercury, the dominant error for models QTD and Lunar is truncation error; in Lunar+Big3 it accounts for approximately one third of the total, as seen by comparing it with EMS+Big3 (whose integration error is much smaller). The physical modeling error in each case amounts to $\approx 3 \times 10^{-4}$ arcsec/yr—less than 10^{-3} of the 43.0 arcsec per century of general relativistic precession suffered by Mercury's orbit (e.g., Weinberg 1972). This residual error is likely the result of neglected relativistic terms, though we have not attempted to prove this. Venus's case is similar—note in particular how little effect the Big 3 asteroids have on it (compare Lunar and Lunar+Big3). For Earth the error is clearly dominated by limitations of the lunar quadrupole approximation, for those models not resolving the Moon explicitly. Interestingly, the modified value of f used by Varadi et. al (2003) actually *worsens* the Earth-Moon barycenter position over this time interval; in spite of this, long-term accuracy is much improved (see below). Notice also the dramatic improvement in Earth's motion when the Moon is treated explicitly (EMS+Big3 and EMS+J_2). By contrast, the lunar ephemeris produced by these models is rather crude; lunar motion is influenced by a variety of physics—rigid-body dynamics, non-spherical shape terms, tidal dissipation, etc.—not included in our models. Touma & Wisdom (1994) discuss the formulation of rigid-body dynamics as a symplectic map.

For Mars and the giant planets, asteroids are the limiting factor. Adding the Big 3 (Ceres,

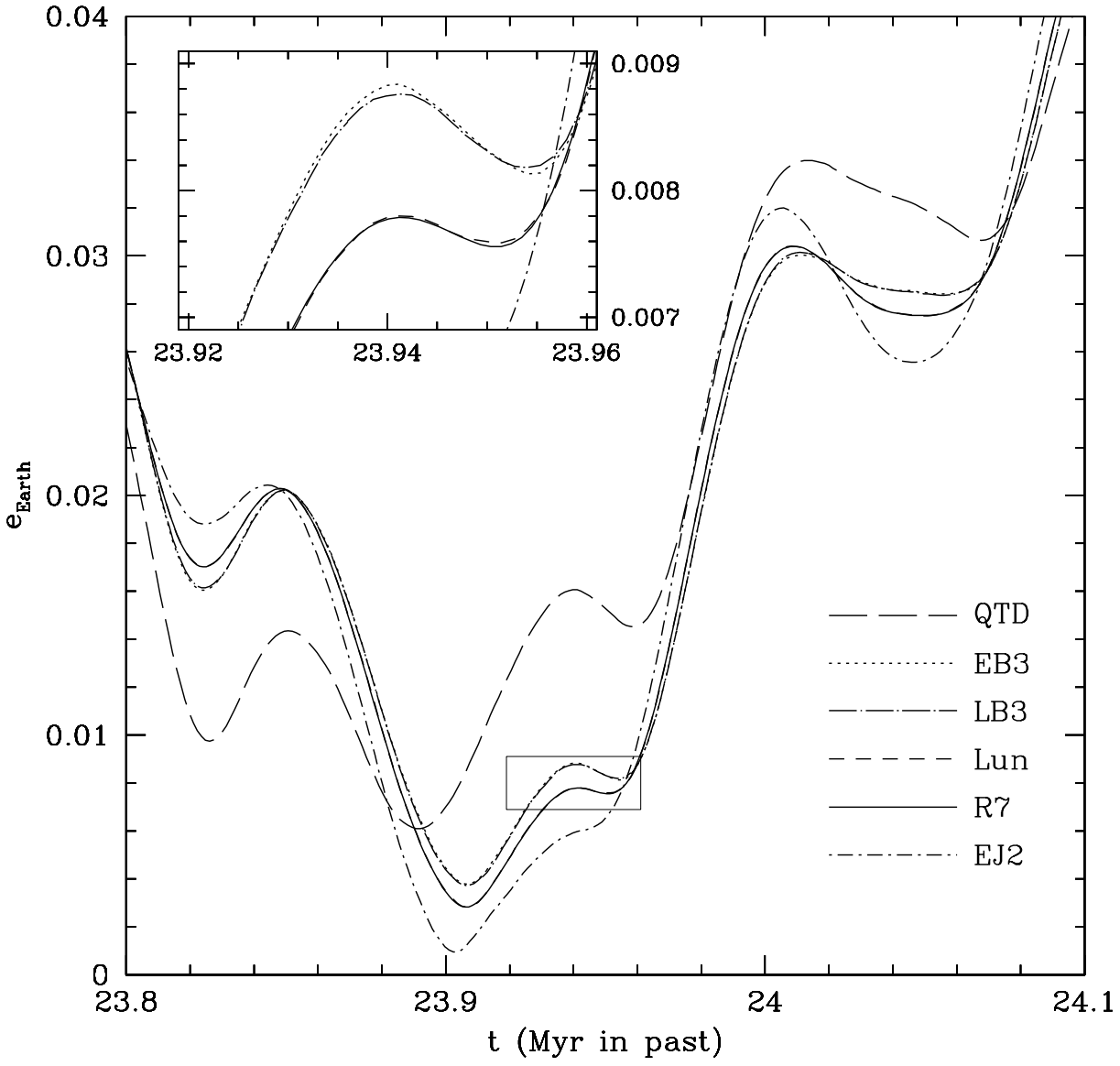

Fig. 1.— See caption section at end of text.

Pallas, and Vesta) reduces the error in Mars by nearly a factor of two, and in the giant planets by an order of magnitude. Although the potential of the asteroid belt is too "grainy" to be accurately modeled as a smooth potential (Standish & Fienga (2002)), we can make a rough estimate of its importance by treating it as a ring of matter. For simplicity, assume a circular ring and circular, co-planar planetary orbits....

4. DISCUSSION

We thank Matthew Holman, Jack Wisdom, Ferenc Varadi, and Hal Levison for helpful discussions. Examination of model EMS+J_2 (§3.4.1) was motivated by an early draft of Varadi et al. (2003). This work was supported by NASA Origins Grant .

A. COMPUTATIONAL DETAILS

A.1. Earth-Moon-Sun Integrations

REFERENCES

Applegate, J.H., Douglas, M.R., Gürsel, Y., Sussman, G.J., & Wisdom, J. 1986, AJ, 92, 176

Goldberg, D. 1991, ACM Computing Surveys, 23, 5

Marsden, J.E., Patrick, G.W., & Shadwick, W.F. (eds.) 1996, Integration Algorithms and Classical Mechanics, Fields Institute Communications, Vol. 10

Mikola, S. 1997, Celest. Mech. Dyn. Ast., 67, 145

Pijpers, F.P. 1998, A&A, 297, 76

Pireaux, S., & Rozelot, J.-P. 2003, Ap&SS, 284, 1159

Press, W. H., Teukolsky, S. A., Vetterling, W. T., & Flannery, B. P. 1992, Numerical Recipes in C (2nd ed.; Cambridge: CUP)

Quinn, T.R., Tremaine, S., & Duncan, M. 1991, AJ, 101, 2287

Rauch, K.P., & Holman, M. 1999, AJ, 117, 1087

Roxburgh, I.W. 2001, A&A, 377, 688

Standish, E.M. 1998, JPL Planetary and Lunar Ephemerides, DE405/LE405, JPL IOM 312.F-98-048

Standish, E.M. 2003, JPL Planetary Ephemeris DE410, JPL IOM 312.N-03-009

Standish, E.M., & Fienga, A. 2002, A&A, 384, 322

Sussman, G.J., & Wisdom, J. 1988, Science, 241, 433

Sussman, G.J., & Wisdom, J. 1992, Science, 257, 56

Touma, J., & Wisdom, J. 1994, AJ, 107, 1189

Varadi, F., Runnegar, B., & Ghil, M. 2003, ApJ, 592, 620

Weinberg, S. 1972, Gravitation and Cosmology (John Wiley & Sons: New York), p. 198

Yoshida, H. 1990, Phys. Lett. A, 150, 262

This preprint was prepared with the AAS LaTeX macros v5.2.

Figure Captions

Fig. 1.— Earth's eccentricity at the Oligocene-Miocene boundary for several models (cf. Table 1) computed by HNBody; models are listed in the same order their curves appear (top to bottom) at time 23.94 Myr. Model R7 from Varadi, Runnegar, & Ghil (2003)—a best-of-class Störmer method calculation—is included for reference (cf. their Figure 1). Model Lun (Lunar) duplicates the physics of R7 using HNBody, and produces virtually identical results. The close agreement between models LB3 (Lunar+Big3) and EB3 (EMS+Big3) confirms the efficacy of the lunar quadrupole term advocated by Varadi et al. (2003). Model QTD duplicates Lunar except that the lunar model of Quinn et al. (1991) is used, and shows the variations induced by a 10% change in the magnitude of the lunar quadrupole term. Model EJ2 (EMS+J_2) demonstrates the influence of a non-zero solar quadrupole moment. The inset box displays a close-up of the indicated portion of the figure.

Table 1. Long-Term Solar System Simulations

Model[a]	Length[b] (Myr)	Stepsize[c] (d)	$\lvert\Delta E/E\rvert$[d]	Asteroids[e]	Lunar model[f]	Solar model
QTD	-25	4	4.0×10^{-12}	$\cdots$	$f = 0.9473$	point mass
Lunar	-25	3	1.1×10^{-12}	$\cdots$	$f = 0.8525$	point mass
Lunar+Big3	$\pm$5400	1.8	2.8×10^{-12}	Big 3	$f = 0.8525$	point mass
EMS+Big3	$\pm$100	1.5	6.2×10^{-13}	Big 3	explicit	point mass
EMS+J_2	-25	1.5	2.7×10^{-13}	$\cdots$	explicit	$J_2 = 2 \times 10^{-7}$

[a]In addition to the effects listed here, all models include the nine planets and first-order general relativistic corrections due to the Sun.

[b]Negative values denote integrations into the past, positive values into the future.

[c]The EMS models used a fourth-order mapping; the others were second-order.

[d]Maximum relative energy error recorded during the simulation.

[e]Big 3 $\equiv$ Ceres, Pallas, and Vesta.

[f]See text for the meaning of f. The QTD lunar model also includes recession of the Moon due to tidal dissipation (the others do not).

Table 2. Solar System Simulation Accuracies[a]

	QTD		Lunar		Lunar+Big3		EMS+Big3		EMS+J_2	
Body	$\alpha^{\rm b}$	$\beta^{\rm b}$	α	β	α	β	α	β	α	β
Mercury	-1.1	0.01	-0.65	0.02	-0.45	0.01	-0.31	0.02	0.22	0.02
Venus	0.05	0.03	0.05	0.03	0.04	0.03	0.03	0.03	0.10	0.03
Earth	4.1	0.02	10.2	0.02	10.2	0.02	0.03	0.01	0.02	0.01
Moon	···	···	···	···	···	···	-7000	1200	-7000	1200
Mars	1.0	0.00	1.0	0.00	0.6	0.00	0.6	0.00	1.0	0.00
Jupiter	-0.12	-0.02	-0.12	-0.02	0.01	-0.01	0.01	-0.01	-0.12	-0.01
Saturn	-0.06	0.00	-0.06	0.00	0.002	0.00	0.002	0.00	-0.06	0.00
Uranus	0.005	0.00	0.005	0.00	0.003	0.00	0.003	0.00	0.004	0.00
Neptune	-0.03	0.00	-0.03	0.00	-0.002	0.00	-0.002	0.00	-0.03	0.00
Pluto	0.005	0.003	0.005	0.003	0.001	0.000	0.001	0.000	0.005	0.003

[a]Positional accuracy relative to the DE 406 ephemeris over the interval 3000 B.C. to 3000 A.D. Planet positions refer to the barycenter of the planet and its satellites (if any); the Moon's position is geocentric.

[b]Parameters α (given in $10^{-3}\,''\,{\rm yr}^{-1}$) and β (given in $10^{-6}\,''\,{\rm yr}^{-2}$) are defined by the relation $\mathrm{sign}(\delta\mathbf{X}\cdot\mathbf{V})\,|\delta\mathbf{X}/\mathbf{X}| \approx \alpha(t-t_0)+\beta(t-t_0)^2$, where $\delta\mathbf{X} = \mathbf{X}-\mathbf{X}_{406}$ is the error in position compared to DE 406, t is the epoch of observation, and t_0 = JD 2440400.5 is the initial epoch. See text for details.